Photochemistry of Methylglyoxal in the Vapor Phase

Stephan Koch* and Geert K. Moortgat

Max-Planck-Institut für Chemie, Atmospheric Chemistry Division, Postfach 3060, 55020 Mainz, Germany

Received: April 17, 1998; In Final Form: July 1, 1998

The photolysis of methylglyoxal (CH_3COCHO) in the presence of synthetic air was studied by laboratory experiments in a static reactor in order to determine its atmospheric lifetime. Quantum yields of the molecular photolysis products CO and HCHO were determined at 298 K as a function of wavelength ($260 \leq \lambda \leq 440$ nm) and pressure ($30 \leq P \leq 900$ Torr) using an optical resolution of 8.5 nm. The results can be distinguished with respect to both UV/VIS-absorption bands of methylglyoxal. For the short-wavelength band ($260 \leq \lambda \leq 320$ nm) photolysis quantum yields were found to be unity, independent of wavelength and pressure, consistent with a dissociation mechanism yielding peroxy radicals and CO according to $CH_3COCHO \xrightarrow{h\nu} \xrightarrow{O_2,M} CH_3COO_2 + HO_2 + CO$ (P1). For the long-wavelength band ($380 \leq \lambda \leq 440$ nm) two different processes were distinguished. The major process is photodissociation (P1) with quantum yields (ϕ_D) decreasing with increasing wavelength and pressure following the Stern−Volmer relationship: $1/\phi_D(\lambda) = 1/\phi_0(\lambda) + P/k'_D(\lambda)$ with $\phi_0(\lambda) = (8.15 \pm 0.5)(10^{-9})$ [exp(7131 ± 267)] nm/λ and $k'_D(\lambda) = (7.34 \pm 0.1)(10^{-9}$ Torr) [exp(8793 ± 300)] nm/λ. The minor process could be described by an H-atom transfer between electronically excited MG and ground-state MG, yielding the experimentally observed products $[CH_3COCHO]^* + CH_3COCHO \xrightarrow{O_2,M} CH_3COO_2 + HCHO + CO + CH_3COO_2$ (R10). The atmospheric lifetime due to photolysis (τ_{phot}) was calculated using an atmospheric radiation model and the above expression, where $\phi_0(\lambda) = 1$ for $\lambda < 380$ nm, resulting in $\tau_{phot} = (4.1 \pm 0.7)$ h for a solar zenith angle of 50° at ground level. Therefore, photolysis can be identified as the most important degradation process of atmospheric methylglyoxal.

Introduction

Methylglyoxal (CH_3COCHO) is an atmospherically important bicarbonyl compound since it is a major product of natural isoprene oxidation. The oxidation of isoprene by OH radicals[1−3] as well as O_3[4−6] leads, besides other products, to the formation of methyl vinyl ketone and methacrolein, which are further oxidized by OH[7,8] or O_3[4,9] to methylglyoxal and other products. Methylglyoxal (MG) is also a product of the OH initiated oxidation of hydroxy acetone.[10,11] In anthropogenically polluted air, MG may be formed by the oxidation of toluene, undergoing ring cleavage after OH attack.[12−14]

Because MG is potentially an atmospheric important precursor of HO_2, CH_3COO_2 radicals, and peroxyacetylnitrate (PAN),[15] it has recently been observed in field experiments, where atmospheric mixing ratios of 50 pptv were detected.[16,17]

The low concentrations of MG in the troposphere are due to efficient degradation pathways by photolysis,[19,20] OH reaction,[21] and dry and wet deposition. NO_3 as well as O_3 reactions are atmospherically not relevant.[22,23] No quantitative data are available concerning the efficiency of the deposition processes.

Photolysis (P1a) and OH reaction (R1) lead, following O_2 addition, to the formation of CO (R2, R3), acetyl peroxy radicals (R4), and HO_2 radicals (R3).[24]

$$CH_3COCHO \xrightarrow{h\nu} CH_3CO + HCO \qquad \text{(P1a)}$$

$$CH_3COCHO + OH \rightarrow CH_3COCO + H_2O \qquad \text{(R1)}$$

$$CH_3COCO \rightarrow CH_3CO + CO \qquad \text{(R2)}$$

$$HCO + O_2 \rightarrow HO_2 + CO \qquad \text{(R3)}$$

$$CH_3CO + O_2 \xrightarrow{M} CH_3COO_2 \qquad \text{(R4)}$$

The reactions of the intermediately formed peroxy radicals give rise to the experimentally observed stable products CO and HCHO as discussed below.

The lifetime due to OH reaction can be estimated to be 16 h for an OH concentration of 1×10^6 molecules cm^{-3} and a room temperature rate coefficient of $k_3 = 1.3 \times 10^{-11}$ cm^3 molecule^{-1} s^{-1}.[21]

The photolysis of MG was already the subject of several laboratory investigations, resulting in estimates of the atmospheric lifetime to 2,[23] 0.6,[19] and 2.7 h ± 0.7 h,[20] respectively.

The lifetime given by Plum et al.,[23] is based on an environmental chamber study by use of an unfiltered Xe arc lamp to simulate the solar spectrum. They also determined adsorption cross sections that were half as large as the values found by Meller et al.[10] and Staffelbach et al.[20]

In the laboratory studies published by Raber and Moortgat,[18,19] the photolysis of MG in the presence of 50−760 Torr synthetic air was investigated using two types of broad-band emitting light sources (275−380 and 390−470 nm) and FTIR detection. From the analysis of the photolysis products (CO, CO_2, HCHO, CH_3OH, CH_3O_2H, HCOOH, CH_3COOH, CH_3COO_2H, CH_3CHO (275−380 nm), O_3, H_2O, $CH_3COCOOH$), the major photodissociation mechanism P1a could be proposed and the

* Author to whom correspondence should be addressed. E-mail: koch@mpch-mainz.mpg.de.

10.1021/jp981915r CCC: $15.00
Published on Web 10/21/1998

atmospheric lifetime was estimated from the average photolysis quantum yield over the lower-wavelength range. Methodologically similar experiments were presented by Staffelbach et al.[20] They investigated the photolysis products of MG in 20 Torr O_2 and 740 Torr N_2 using the light of a Xe arc lamp in conjunction with several broad-band filters (410−418, 355−480, 280−420, 280−420, and 240−420 nm) and FTIR detection. The photolysis products found by Raber and Moortgat (except CH_3CHO, CH_3O_2H, and $CH_3COCOOH$) and the major dissociation mechanism were confirmed by Staffelbach et al., but a five times larger atmospheric lifetime was determined from their quantum yields.

With respect to the discrepancies and the insufficiencies of the broad-band quantum yields determined in earlier experiments, the quantitative determination of the quantum yields of the photolysis of MG as a function of wavelength and pressure were necessary in order to obtain reliable information on the atmospheric lifetime of MG. Therefore, the quantum yields of the molecular photolysis products CO and HCHO were investigated in order to derive quantitative information about the primary photodissociation processes.

Experimental Section

Experiments were performed in a static reactor made of a piece of Pyrex tubing of 100 mm length and 35 mm inner diameter, fitted with double-sided evacuated quartz windows on both ends. The inner surface of the reactor had to be deactivated by silanization with hexamethyldisilazan (HMDS) at 650 K[25] in order to minimize adsorption of MG on the reactor walls, since in earlier experiments a significant amount of the products observed were due to photolysis of MG adsorbed on the reactor walls.

$$\sim\mathrm{Si{-}O{-}H} + \frac{1}{2}\mathrm{H{-}N(-Si(-CH_3)_3)_2} \xrightarrow{650\ \mathrm{K}} \sim\mathrm{Si{-}O{-}Si(CH_3)_3} + \frac{1}{2}\mathrm{NH_3}\uparrow$$

As light source a 150 W Xe arc lamp (Cermax LX150 UV) equipped with a parabolic reflector was used, emitting a continuous spectrum (240−800 nm) without sharp maxima. The nearly parallel light beam was focused with a quartz lens (f = 120 mm) onto the entrance slit (5 mm) of a f/2 monochromator (Jobin-Yvon H.L.) equipped with a 1484 grooves/mm grating. The divergent light cone was made parallel by a lens (f = 120 mm) and passes through the reactor with little illumination of the side walls. The photon flux was registered with a manufacturer-calibrated photodiode (Newport 818 UV with attenuator), and the digitized signals were stored in a computer. The spectral resolution of the optical set-up was determined using a second monochromator (AMKO Metrospec, 1200 grooves/mm, slit width 0.5 mm) to be 8.5 ± 0.1 nm FWHM of an almost Gaussian distribution.

The gaseous mixtures (0.03−1 Torr MG, 30−900 Torr synthetic air) to be photolyzed were prepared in a mixing system equipped with capacitance manometers (MKS Baratron, 10 and 1000 Torr range) and expanded into the evacuated reactor.

Samples were taken in intervals of 5 min, by expansion of the gas mixture into an evacuated sample loop consisting of a 1 m, 0.5 mm i.d. deactivated fused silica capillary connected to a six-port valve (Valco) which served as a splitless injector. Each sampling step reduced the pressure in the reactor by 0.85% ± 0.05% which had to be taken into account when calculating photochemical yields.

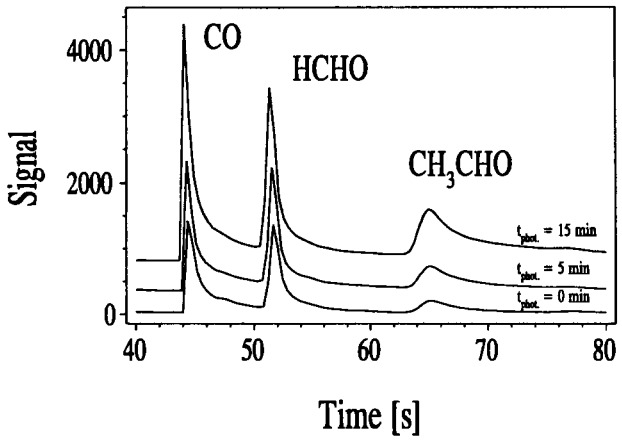

Figure 1. Chromatograms of photolysis mixtures ([MG] = 5.3×10^{15} molecules cm^{-3}, 300 Torr synthetic air, 280 nm) recorded after different photolysis times, using the RGD.

Samples were analyzed using a gas chromatograph (Hewlett Packard 5890) equipped with a flame ionization detector (FID), a quadrupole mass selective detector (HP 5970 MSD), and a reduction gas detector (Trace Analytical RGD 2). Samples to be analyzed with the reduction gas detector (RGD) or the FID were isothermally separated within 80 s (Figure 1) on a 60 m, 0.5 mm i.d. quartz capillary column coated with a 5 μm poly-methylsiloxane phase (Quadrex 007) with a He carrier gas flow rate of about 60 mL/min. The MSD was connected directly to a 30 m, 0.25 mm i.d. column (1 μm poly-methylsiloxane, J&B 5) using a flow rate of 0.8 mL/min.

Quantitative detection of the photolysis products CO, HCHO, and CH_3CHO was performed with the reduction gas detector (RGD) which is particularly selective and sensitive for CO and carbonyl compounds. Yellow HgO in a stainless steel tube of 35 mm length and 4 mm i.d. is reduced by CO and carbonyls at 550 K to Hg vapor which is detected by absorption of the 254 nm line of a Hg lamp.

$$\mathrm{CO} + \mathrm{HgO} \xrightarrow{550\ \mathrm{K}} \mathrm{CO_2} + \mathrm{Hg}\uparrow$$

$$\mathrm{HCHO} + 2\mathrm{HgO} \xrightarrow{550\ \mathrm{K}} \mathrm{CO_2} + \mathrm{H_2O} + \mathrm{Hg}\uparrow$$

Due to adsorption of analytes on the HgO surface, peak tailing (Figure 1) and saturation effects were observed. The signals were digitized and integrated on a computer.

The specified purities of the gases used in the photolysis experiments and for chemical actinometry were, if not stated otherwise, 99.999%: He, synthetic air, N_2, O_2, H_2, CO 99.997%, Cl_2 99.96%, CH_4 99.95%, C_2H_6 99.95%. The carrier gas was further purified by use of filter cartridges with respect to traces of CO, O_2, and hydrocarbons.

Acetaldehyde was obtained with a purity of 99% and degassed by repeated trap-to-trap distillation. Formaldehyde was prepared by gentle heating of paraformaldehyde (95%), and traces of water and oligomers were removed using a cold trap at 170 K.

Methylglyoxal, obtained as a 40% solution in water, was concentrated by pumping off the water for several hours. The resulting high-viscous polymer was distilled at 330 K and 10^{-3} Torr over a column of 300 mm length and 30 mm i.d. packed with phosphorus pentoxide (98%).[10] The freshly prepared MG still contained impurities of CO (<2%), HCHO (<0.5%), CH_3CHO (<0.5%), and traces of biacetyl and pyruvic acid which were identified by their mass spectra. Although CO, HCHO, and CH_3CHO were also found as photolysis products (Figure 1), their concentration also increased during storage in the dark. A 5% decomposition of the sample as determined by

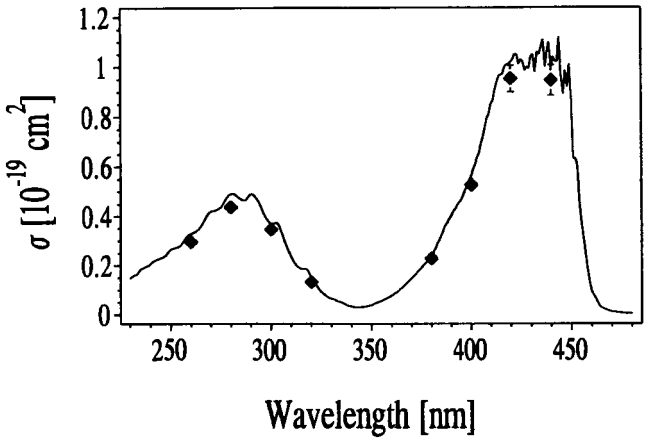

Figure 2. Absorption spectrum of MG. Symbols: cross sections determined in this work, at a resolution of 8.5 nm. Line: high-resolution spectrum.[10]

the CO production, occurred within a period of several hours to several weeks. Therefore, the MG used in experiments was freshly distilled from the polymer, as the accuracy of the product yield determination was limited by the amount of impurities, not by the sensitivity of detection.

Actinometry

The photodissociation of a molecule is generally described by a first-order kinetic process with the photodissociation coefficient (k_{phot}) given as an integral over the observed wavelength range,

$$k_{phot}(P) = \int \phi(\lambda, P)\, I_0(\lambda)\, \sigma(\lambda)\, d\lambda \qquad (1)$$

where ϕ represents the quantum yield of the process, I_0 the photon flux per unit wavelength, and σ the absorption cross section. Under the assumption that these parameters do not change significantly, the integral can be substituted by mean values (eq 2) as it was done in this work.

$$\bar{k}_{Prod}(\lambda_0, P) = \bar{\phi}(\lambda_0, P)\, \bar{\sigma}(\lambda_0) \int I_0(\lambda)\, d\lambda \qquad (2)$$

The photon flux ($\int I_0(\lambda)\, d\lambda$) was determined as a function of wavelength using Cl_2 as gaseous chemical actinometer, as it can be used in the same apparatus as used in the MG experiments. Molecular chlorine photodissociates with quantum yields of unity and shows sufficiently large cross sections in the wavelength range of interest ($260 < \lambda < 440$ nm).[26]

Absorption Cross Sections. The absorption cross sections were determined at 298 K in the wavelength range between 260 and 440 nm in intervals of 20 nm with the same experimental set-up and the same optical resolution as used in the photolysis experiments. The cross sections of Cl_2 were obtained with a relative precision of 2% but were somewhat lower (≈2%) than the values reported in the literature,[26] which is expected due to the lower resolution used in this work.

The UV/VIS absorption spectrum of MG, consisting of two absorption bands (Figure 2), determined by Meller et al.[10] and Staffelbach et al.[20] were in very good agreement. The short-wavelength band ($\lambda < 340$ nm) is assigned by an electronically $n_- \rightarrow \pi_4$ transition, the long-wavelength band ($\lambda > 340$ nm) by a $n_+ \rightarrow \pi_3$ transition.[27,28]

The absorption cross sections found for MG, displayed in Figure 2, are systematically about 10% lower than given in the literature.[10,20] This discrepancy can be explained by heterogeneous losses of MG, as reported by Meller et al.[10] The relative statistical errors in the determination of the cross sections were found to be ±6% and are caused by the uncertainty of the MG concentration.

Photon Flux. Mixtures of C_2H_6 (5×10^{13} to 5×10^{14} molecules cm^{-3}) and Cl_2 in at least 10-fold excess (5×10^{14} to 9×10^{15} molecules cm^{-3}) in 760 Torr synthetic air were photolyzed at 298 K to an amount of ca. 10% removal of C_2H_6. The decay of ethane was monitored by use of the FID, and the results were numerically fitted to the kinetic model shown in Table 1 using Facsimile.[29] The photon flux ($\int I_0(\lambda)\, d\lambda$) obtained at the selected wavelengths was in the range between $(0.81 \pm 0.07) \times 10^{14}$ photons $cm^{-2}\ s^{-1}$ at 260 nm and $(3.84 \pm 0.22) \times 10^{14}$ photons $cm^{-2}\ s^{-1}$ at 440 nm. The relative statistical error

TABLE 1: Reactions of the Ethyl Peroxy Radical

		$k(298)$ [$cm^3\ s^{-1}$]	ref
$Cl + C_2H_6$	$\xrightarrow{O_2, M}$ $C_2H_5O_2 + HCl$	$(5.9 \pm 0.3)\ 10^{-11}$	24
$C_2H_5O_2 + C_2H_5O_2$	$\longrightarrow$ $C_2H_5OH + CH_3CHO + O_2$	$(4.4 \pm 0.8)\ 10^{-14}$	41
	$\xrightarrow{O_2, M}$ $2CH_3CHO + 2HO_2$	$(2.3 \pm 0.4)\ 10^{-14}$	41
$HO_2 + C_2H_5O_2$	$\longrightarrow$ $C_2H_5O_2H + O_2$	$(5.4 \pm 1.0)\ 10^{-12}$	42, 43
$Cl + C_2H_5OH$	$\xrightarrow{O_2, M}$ $CH_3CHO + HCl + HO_2$	$(9.4 \pm 1.0)\ 10^{-11}$	24
$Cl + CH_3CHO$	$\xrightarrow{O_2, M}$ $CH_3COO_2 + HCl$	$(7.2 \pm 1.0)\ 10^{-11}$	24
$Cl + C_2H_5O_2H$	$\xrightarrow{O_2, M}$ products + HCl	$(1.1 \pm 0.2)\ 10^{-10}$	44

TABLE 2: Reactions of the Acetyl Peroxy Radical

		$k(298)$ [$cm^3\ s^{-1}$]	ref
$CH_3COO_2 + CH_3COO_2$	$\xrightarrow{O_2, M}$ $2CH_3O_2 + 2CO_2$	$(1.4 \pm 0.2)\ 10^{-11}$	45
$CH_3O_2 + CH_3COO_2$	$\xrightarrow{O_2, M}$ $CH_3O_2 + CO_2 + HCHO + HO_2$	$(8.8 \pm 1.5)\ 10^{-12}$	45
	$\longrightarrow$ $HCHO + CH_3COOH + O_2$	$(1.0 \pm 0.5)\ 10^{-12}$	45
$HO_2 + CH_3COO_2$	$\longrightarrow$ $CH_3COO_2H + O_2$	$(8.5 \pm 4.5)\ 10^{-12}$	46
	$\longrightarrow$ $CH_3COOH + O_3$	$(2.9 \pm 0.7)\ 10^{-12}$	46
$HO_2 + CH_3O_2$	$\longrightarrow$ $CH_3O_2H + O_2$	$(5.2 \pm 0.3)\ 10^{-12}$	24
$HO_2 + HO_2$	$\longrightarrow$ $H_2O_2 + O_2$	$(1.6 \pm 0.2)\ 10^{-12}$	24
	$\xrightarrow{M}$ $H_2O_2 + O_2$	$(1.6 \pm 0.2)\ 10^{-13}$ [a]	24

[a] 100 Torr synthetic air.

in the determination of the photon flux is ±7% and is caused by the error of $d[C_2H_6]/dt$. Possible systematic errors, introduced by uncertainties of the reaction rates (Table 1), were estimated to affect the results not more than 3%. The output of the lamp was monitored during each experiment and corrected for long-term fluctuations.

Results and Discussion

Depending on the energy of the photon absorbed, the following thermodynamically allowed pathways of dissociation of electronically excited MG are possible.

$$CH_3COCHO \xrightarrow{h\nu} CH_3CO + HCO \ (\lambda < 422 \text{ nm}) \quad \text{(P1a)}$$

$$\xrightarrow{h\nu} CH_3COCO + H \ (\lambda < 385 \text{ nm}) \quad \text{(P1b)}$$

$$\xrightarrow{h\nu} CH_3 + COCHO \ (\lambda < 370 \text{ nm}) \quad \text{(P2a)}$$

$$\xrightarrow{h\nu} CH_3 + CO + HCO \ (\lambda < 343 \text{ nm}) \quad \text{(P2b)}$$

$$\xrightarrow{h\nu} CH_3CHO + CO \ (\text{all } \lambda) \quad \text{(P3)}$$

$$\xrightarrow{h\nu} CH_3CHO + CO \ (\text{all } \lambda) \quad \text{(P3)}$$

The threshold wavelengths were calculated from enthalpy data ($\Delta H_f^\circ(298)$).[24,30] However, considering that the mean enthalpy of vibration and rotation is 2.5 kJ/mol (200 cm^{-1}) per degree of freedom, it follows that P1a is thermodynamically allowed at all wavelengths investigated in this study.

The primary steps P1a and P1b cannot be distinguished in the presence of O_2, since their primary products yield by fast reactions the same peroxy radicals (R3, R4 and R2, R5, respectively). P2a and P2b are also indistinguishable and yield two molecules of CO per molecule dissociated (R7, R3).

$$HCO + O_2 \xrightarrow{M} HO_2 + CO \quad \text{(R3)}$$

$$CH_3CO + O_2 \xrightarrow{M} CH_3COO_2 \quad \text{(R4)}$$

$$CH_3COCO \rightarrow CH_3CO + CO \quad \text{(R2)}$$

$$H + O_2 \xrightarrow{M} HO_2 \quad \text{(R5)}$$

$$CH_3 + O_2 \xrightarrow{M} CH_3O_2 \quad \text{(R6)}$$

$$COCHO \xrightarrow{M} CO + HCO \quad \text{(R7)}$$

The formation of HCHO and other molecular and intermediate radical products are expected due to the known peroxy radical reactions given in Table 2.

Therefore, in principle, the primary dissociation pathways (P1−P4) can be quantitatively distinguished by examining the quantum yields of the molecular photolysis products CO, HCHO, CH_3CHO, and CH_4.

Product Quantum Yields in Synthetic Air. Mixtures of MG (1×10^{15} to 1×10^{16} molecules cm^{-3}) in 30−900 Torr of synthetic air were photolyzed for up to 60 min, consuming not more than 5% of the initial MG, at 298 K and wavelengths between 260 and 440 nm. CO, HCHO, and CH_3CHO could be detected as products with the RGD. Relatively large amounts of MG as used in these experiments led to saturation of the detector; therefore, the initial concentrations of methylglyoxal could only be quantified volumetrically.

The product quantum yields (ϕ_{Prod}) were derived from the slope of the concentration−time profiles (d[Prod]/dt), which were linear in all cases.

$$\phi_{Prod}(\lambda, P) = \frac{d[Prod]/dt(\lambda, P)}{[MG]_0\, \sigma(\lambda) \int I_0(\lambda)\, d\lambda} \quad (3)$$

The quantum yields of CO, CH_3CHO, and HCHO are displayed in Figures 3, 4, and 5 as a function of the pressure of air (P) for all wavelengths investigated. The error bars represent the standard deviation of the slope of the concentration-time profiles (Δ(d[Prod]/dt)). In separate experiments using the FID, the dark loss of MG to the reactor walls was determined to be $k_{dark} = (2 \pm 1.5) \times 10^{-5}$ s^{-1}, of the same order of magnitude as the photolysis rates of MG. Therefore, dark losses resulted in underestimations of the quantum yields, comparable to of the amount of reaction, less than 5%. The quantum yields can, like the UV/VIS spectrum, be distinguished with respect to both absorption bands, consequently they will be discussed separately.

Short-Wavelength Band (260 ≤ λ ≤ 320 nm). The product quantum yields obtained in this region are independent of wavelength as well as pressure (Figures 3, 4, 5).

$$\phi_{CO}\ (260 \le \lambda \le 320 \text{ nm}) = 1.20 \pm 0.09$$

$$\phi_{HCHO}\ (260 \le \lambda \le 320 \text{ nm}) = 0.19 \pm 0.02$$

$$\phi_{CH_3CHO}\ (260 \le \lambda \le 320 \text{ nm}) = 0.18 \pm 0.04$$

CO and CH_3CHO Quantum Yields. In order to explain the experimentally observed CO quantum yields higher than unity, gas phase processes with yields higher than 1.0 (P2, P4), or heterogeneous photolysis of MG adsorbed onto the reactor walls have to be assumed, since the radical intermediate of P1, CH_3COO_2, does not represent a source of CO (Table 2).

The photodissociation channel P4 can be excluded, since no CH_4 could be detected as photolysis product in experiments (260 ≤ λ ≤ 440 nm) using the FID. Note that, with respect to the detection limit of CH_4, one obtains $\phi_{CH_4} < 0.002$, in accordance with earlier work.[19,20]

Assuming that CO is formed via P1′, P2′, and P3 (eq 4) and that CH_3CHO is produced via P3 (eq 5),

$$CH_3COCHO \xrightarrow{h\nu} \xrightarrow{O_2,M} CH_3COO_2 + HO_2 + CO \quad \text{(P1′)}$$

$$\xrightarrow{h\nu} \xrightarrow{O_2,M} CH_3O_2 + HO_2 + 2CO \quad \text{(P2′)}$$

$$\xrightarrow{h\nu} CH_3CHO + CO \quad \text{(P3)}$$

one obtains under the condition that the sum of primary quantum yields is unity (eq 6) the following equations:

$$\phi_1 + 2\,\phi_2 + \phi_3 = 1.2 = \phi_{CO} \quad (4)$$

$$\phi_3 = 0.2 = \phi_{CH_3CHO} \quad (5)$$

$$\phi_1 + \phi_2 + \phi_3 = 1 \quad (6)$$

with (4) and (5),

$$\phi_1 + 2\phi_2 = 1 \quad (7)$$

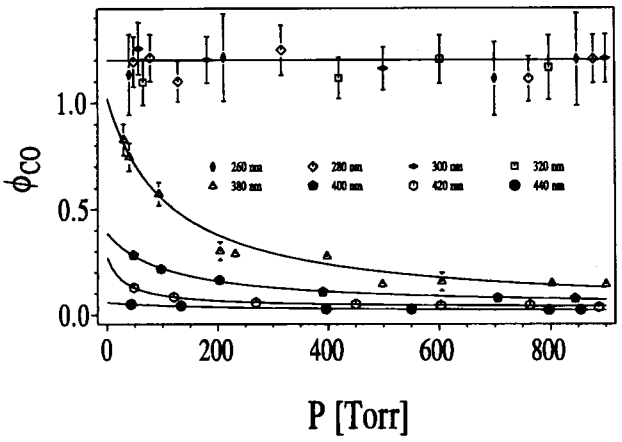

Figure 3. Quantum yields of CO as a function of pressure obtained in synthetic air. Symbols: experimental data at the indicated wavelengths; horizontal line: mean values of experimental data obtained at wavelengths between 260 and 320 nm; curves: fit according to eq 12.

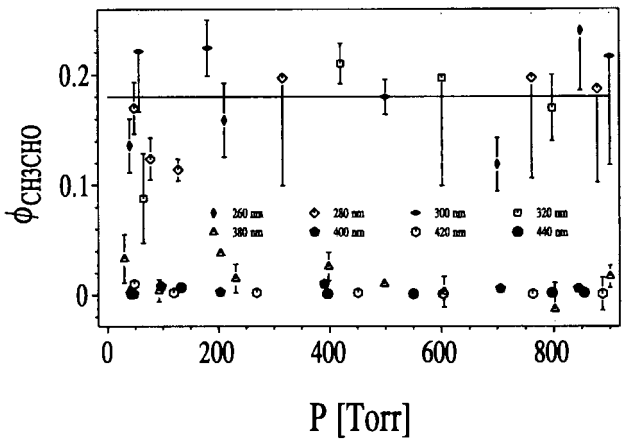

Figure 4. Quantum yields of CH_3CHO as a function of pressure obtained in synthetic air. Symbols: experimental data at the indicated wavelengths; horizontal line: mean values of experimental data obtained at wavelengths between 260 and 320 nm.

with (5) and (6),

$$\phi_1 + \phi_2 = 0.8 \tag{8}$$

with (7) and (8),

$$\phi_1 = 0.6$$

and

$$\phi_2 = 0.2$$

From model calculations of this case, according to the reaction scheme in Table 2, a HCHO quantum yield of 0.15 is expected. However, this explanation is unrealistic for several reasons. Staffelbach et al. did not find CH_3CHO as photolysis product of MG[20] using a stainless steel reactor. On the other hand, Raber and Moortgat, using a reactor made of quartz, observed CH_3CHO with quantum yields of 0.1 when photolyzing MG in the wavelength range between 275 and 380 nm.[19] However, constant and pressure independent quantum yields over the wavelength range 260−320 nm are not expected if they do not correspond to a primary process with a quantum yield of unity.

Also, formation of CO and CH_3CHO via chain reactions of the acetyl radical with MG (R8, R2) can be excluded with respect to the fast reaction with O_2 (R4).

$$CH_3CO + CH_3COCHO \rightarrow CH_3CHO + CH_3COCO \quad \text{(R8)}$$

$$CH_3COCO \rightarrow CH_3CO + CO \quad \text{(R2)}$$

$$CH_3CO + O_2 \xrightarrow{M} CH_3COO_2 \quad \text{(R4)}$$

No oxygen partial pressure dependence of the CH_3CHO quantum yield was observed under the experimental conditions employed in this work.

Assuming that the formation of acetaldehyde is caused by photolysis of MG adsorbed onto the reactor walls

$$(CH_3COCHO)_{wall} \xrightarrow{h\nu} CH_3CHO\uparrow + CO\uparrow$$

the CO quantum yield of the gas phase ($\phi_{CO'}$) is then

$$\phi_{CO'} = \phi_{CO} - \phi_{CH_3CHO} = 1.0 \pm 0.1 \tag{9}$$

This supposition is reasonable with respect to the experimentally observed dark loss of MG. Consequently, the CO quantum yields ($\phi_{CO'}$) mentioned further in the text reflect the experimentally observed CO quantum yields reduced by the CH_3CHO quantum yields (eq 9).

HCHO Quantum Yields. The quantum yields of formaldehyde, initiated by P1, can very well be explained by the reaction sequence of the intermediately formed peroxy radicals, as given in Table 2. Numerical simulation of this system shows a very good agreement between the experimentally observed quantum yield $\phi_{HCHO} = 0.19 \pm 0.02$ and the result of the model calculation (0.21 ± 0.05). The uncertainty of the kinetic model was investigated by repeated random variation of the rate coefficients within their error limits, given in Table 2. The assigned error is the FWHM of the Gaussian-like distribution of the quantum yield obtained after 1000 computations.

Photodissociation of MG yielding 2 equivalents of CO according to P2′

$$CH_3COCHO \xrightarrow{h\nu} \xrightarrow{O_2,M} CH_3O_2 + HO_2 + 2\,CO \quad \text{(P2′)}$$

can be ruled out, since quantum yields of $\phi_{CO} = 2$ and $\phi_{HCHO} = 0.12$ are expected from numerical analysis of the kinetic model in contradiction to the experimental results.

Long-Wavelength Band ($380 \le \lambda \le 440$ nm). The quantum yields of CO and HCHO from the long-wavelength transition increase with the energy of the photon absorbed. The acetaldehyde yields do not exceed 5% of the CO yields, hence they are practically negligible.

CO Quantum Yields. The CO yields decrease with increasing pressure and show in the Stern−Volmer representation a nonlinear relationship between the reciprocal quantum yields and total pressure (Figure 6). These findings can be empirically described, if the experimentally observed quantum yields are assumed as a sum of two independent yields, ϕ_D and ϕ_{CO_∞}.

$$\phi_{CO}(\lambda, P) = \phi_D(\lambda, P) + \phi_{CO_\infty}(\lambda)$$

$$(\phi_{CO})^{-1}(\lambda, P) = \frac{(\phi_D)^{-1}(\lambda, P)}{1 + \phi_{CO_\infty}(\lambda) \times (\phi_D)^{-1}(\lambda, P)} \tag{10}$$

The first term (ϕ_D) is supposed to represent the photodissociation as a function of pressure, obeying the Stern−Volmer relationship

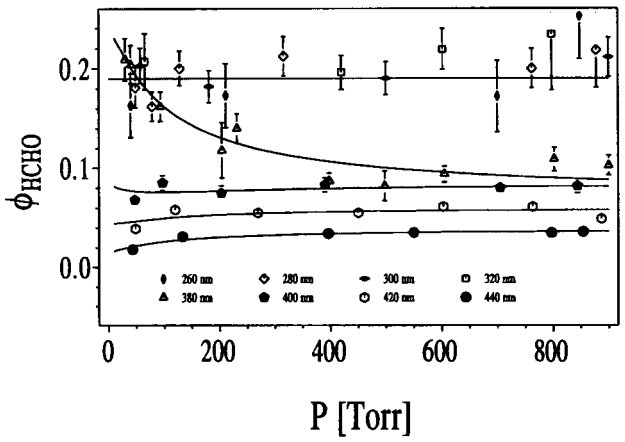

Figure 5. Quantum yields of HCHO as a function of pressure obtained in synthetic air. Symbols: experimental data; horizontal line: mean values of experimental data obtained at wavelengths between 260 and 320 nm.

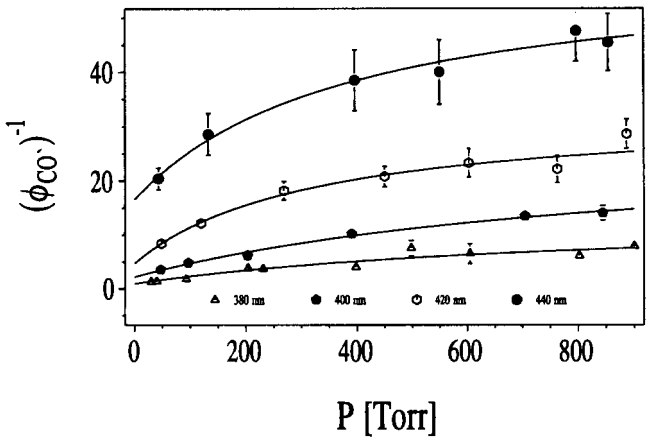

Figure 6. Stern−Volmer representation of reciprocal quantum yields of CO obtained in synthetic air. Symbols: experimental data at the indicated wavelengths; curves: fit according to eq 12.

(eq 11),

$$(\phi_D)(\lambda, P) = \frac{k_D(\lambda)}{k_D(\lambda) + k_X(\lambda) + k_P(\lambda) \times P} = \frac{k'_D(\lambda)}{k'_D(\lambda) + k'_X(\lambda) + P}$$

$$\frac{1}{\phi_D(\lambda, P)} = \frac{1}{\phi_0(\lambda)} + \frac{P}{k'_D(\lambda)} \qquad (11)$$

with

$$\frac{1}{\phi_0(\lambda)} = 1 + \frac{k'_X(\lambda)}{k'_D(\lambda)}$$

where k_D, k_X, und k_P represent the rate coefficients of dissociation, the pressure-independent, and the pressure-dependent deactivation of vibronically excited molecules. The coefficients k'_D und k'_X are normalized to k_P, and ϕ_0 indicates the quantum yield extrapolated to zero pressure. The minor yield (ϕ_{CO_∞}) is assumed to be pressure independent, giving the limit of the CO quantum yield at infinite pressure. Substituting eq 11 in eq 10 yields the expression of $(\phi_{CO})^{-1}$ as a function of pressure as

TABLE 3: Coefficients of CO Quantum Yield According to Equation 12

λ[nm]	ϕ_0	ϕ_{CO_∞}	k'_D [Torr]
380	1.10 ± 0.12	0.043 ± 0.040	76 ± 21
400	0.37 ± 0.03	0.030 ± 0.013	36 ± 9
420	0.18 ± 0.03	0.030 ± 0.004	9 ± 2
440	0.05 ± 0.01	0.018 ± 0.002	4 ± 1

displayed in Figure 6 with coefficients given in Table 3.

$$(\phi_{CO})^{-1}(\lambda) = \frac{(\phi_0)^{-1} + P/k'_D}{1 + \phi_{CO_\infty}((\phi_0)^{-1} + P/k'_D)} \qquad (12)$$

HCHO Quantum Yields. Quantum yields of formaldehyde increase with photon energy and show at 380 nm little and in the range of 400−440 nm no dependence upon pressure (Figure 5). To explain these unusual observations, the quantum yields are, as in the case of CO, assumed to be described by a sum of two functions. If the first term is given by a Stern−Volmer function analogous to eq 11, then the second term must show a positive pressure dependence (in order to compensate the first) so to reach constant values at high pressure, when the contribution of the Stern−Volmer function becomes zero. Therefore, a process has to be postulated which reflects a rate of HCHO formation increasing with pressure and reaching a limit at high pressures.

The rate of the reaction R9

$$CH_3O + O_2 \rightarrow HCHO + HO_2 \qquad (R9)$$

is proportional to the O_2 partial pressure and might therefore appear as a pressure-dependent source of HCHO in experiments performed in synthetic air, since the $[O_2]/P$ ratio is constant. However, quantum yields obtained at wavelengths shorter than 320 nm show no O_2 partial pressure dependence. Therefore, it can be concluded that eventually competing reactions are slow compared to R9 under the experimental conditions employed in this work.

For the intramolecular rearrangement of an H atom

$$CH_3COCHO \xrightarrow{h\nu} H_2C{=}CO + HCHO$$

leading to the formation of ketene and formaldehyde, pressure-dependent quantum yields would be expected since this process represents a photodissociation. No hint of this pressure dependence has been observed in this study or earlier investigations. This is reasonable, since the thermodynamically favored pathway leading to methane (P4) also does not occur.

A reaction path yielding HCHO is feasible via intermolecular H atom transfer between electronically excited MG and ground-state MG, followed by fragmentation of the C−C bond leading to CO, HCHO, and acetyl radicals.

$$[CH_3COCHO]^* + HCOCOCH_3 \rightarrow CH_3CO + HCHO + CO + CH_3CO \qquad (R10)$$

A comparable gas phase reaction was observed by the photofragmentation of 2-pentanone. This Norrish Type II reaction proceeds via formation of a biradical intermediate undergoing an intramolecular H shift, followed by fragmentation of the C−C bond yielding enol-acetone ($CH_3C(OH){=}CH_2$) and ethene as products.[31]

$$CH_3COCH_2CH_2CH_3 \xrightarrow{h\nu} [CH_3C(OH)CH_2CH_2CH_2]^*$$

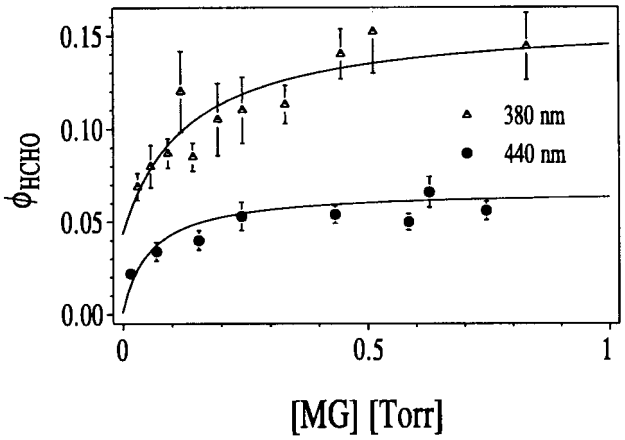

Figure 7. Quantum yields of HCHO as a function of MG concentration (380 nm: $P = 400$ Torr, $[O_2] = 90$ Torr; 440 nm: $P = 760$ Torr, $[O_2] = 150$ Torr). Symbols: experimental data.

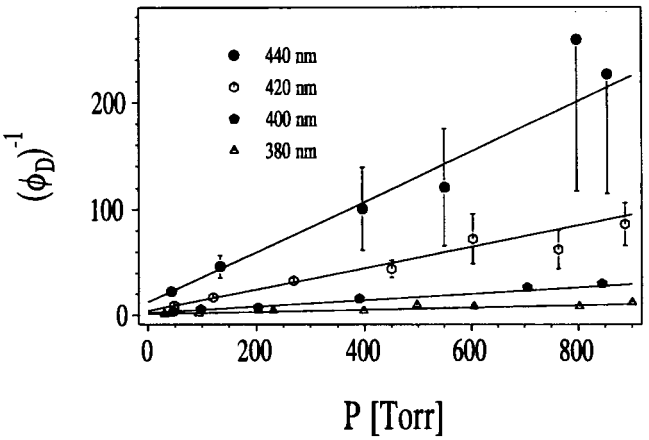

Figure 8. Stern−Volmer representation of reciprocal quantum yields of dissociation obtained in synthetic air. Symbols: calculated from experimental data according to eq 15; curves: fit according to eq 11.

$$[CH_3C(OH)CH_2CH_2CH_2]^* \rightarrow CH_3C(OH)=CH_2 + H_2C=CH_2$$

If reaction R10 occurs, then the yield of HCHO should increase with MG concentration. Testing this hypothesis, further experiments were performed at 380 and 440 nm, under constant pressure and variable MG concentrations. Figure 7 shows the increase of ϕ_{HCHO} with MG concentration reaching a plateau at partial pressures higher than about 1 Torr. This experiment clearly demonstrates the dependence of the HCHO quantum yields on MG concentration; however, no information concerning the total pressure dependence is obtained. Therefore, further experiments were performed in order to verify this approach.

Elementary Processes

Supposing that in the long-wavelength band the experimentally observed yields are caused by two different processes, photodissociation (P1a) and chemical reaction of electronically excited MG (R10), then the CO and HCHO quantum yields represent a linear combination of the quantum yields of both elementary processes, ϕ_D and ϕ_R,

$$\phi_{CO} = \alpha\phi_D + \gamma\phi_R \quad (13)$$

$$\phi_{HCHO} = \beta\phi_D + \delta\phi_R \quad (14)$$

where the coefficients α, β, γ, and δ represent the relative product yields of each process. If these coefficients are known, the quantum yields ϕ_D and ϕ_R can be extracted from the experimentally observed quantum yields.

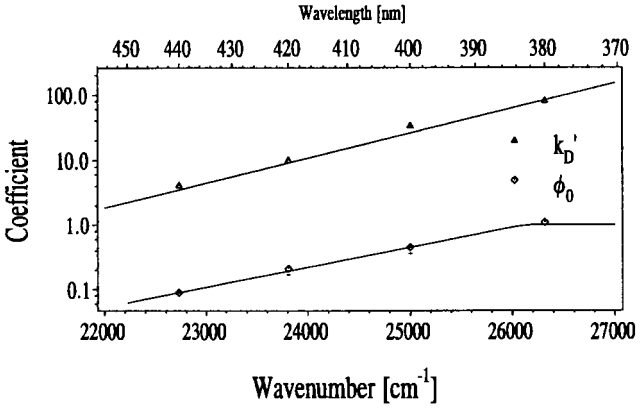

Figure 9. Coefficients of quantum yield of dissociation as a function of reciprocal wavelength. Symbols: coefficients as given in Table 4; lines: fit according to eqs 17 and 18, respectively.

$$\phi_D = (\delta\phi_{CO'} - \gamma\phi_{HCHO})\,\epsilon \quad (15)$$

$$\phi_R = (\alpha\phi_{HCHO} - \beta\phi_{CO'})\,\epsilon \quad (16)$$

with

$$\epsilon = (\alpha\delta - \beta\gamma)^{-1}$$

The relative product yields can be predicted by numerical analysis of the reaction scheme given in Table 2. For the dissociation yield via P1a, one obtains $\alpha = 1.00 \pm 0.00$ and $\beta = 0.21 \pm 0.06$, which means that per molecule dissociated, one molecule of CO as well as 0.2 molecules of HCHO are formed. These results agree with the quantum yields obtained at short wavelengths. The coefficients due to R10 were calculated using the reactions given in Table 2, $\gamma = 1.00 \pm 0.00$ and $\delta = 2.03 \pm 0.03$ with $\epsilon = 0.55 \pm 0.02$. The assigned errors were estimated regarding the uncertainties of the rate coefficients of the peroxy radical reactions. By variation of the boundary conditions it was found that the values of the coefficients α, β, γ, and δ do not change significantly, if both processes take place simultaneously with variable contributions.

Quantum Yields of Photodissociation. The quantum yields of photodissociation (P1a) were extracted from experimental data according to eq 15. The reciprocal yields are shown as a function of total pressure (P) in Figure 8 and are found to be consistent with linear Stern−Volmer functions (eq 11). The coefficients of these functions are given in Table 4 and are in very good agreement with those in Table 3. The assigned errors represent the standard deviations of the parameters obtained from weighted least-squares fits. The coefficients k_D' and ϕ_0 can also be described by an exponential function of the reciprocal wavelength as shown in Figure 9.

$$k_D'(\lambda) = (7.34 \pm 0.1)(10^{-9}\ \text{Torr})\,[\exp(8793 \pm 300)]\ \text{nm}/\lambda \quad (17)$$

$$\phi_0(\lambda) = (8.15 \pm 0.5)(10^{-9})\,[\exp(7131 \pm 267)]\ \text{nm}/\lambda \quad \text{for } \lambda > 380\ \text{nm} \quad (18)$$

$$\phi_0(\lambda) = 1 \text{ for } \lambda < 380\ \text{nm}$$

Using eq 11 together with the expressions given in eqs 17 and

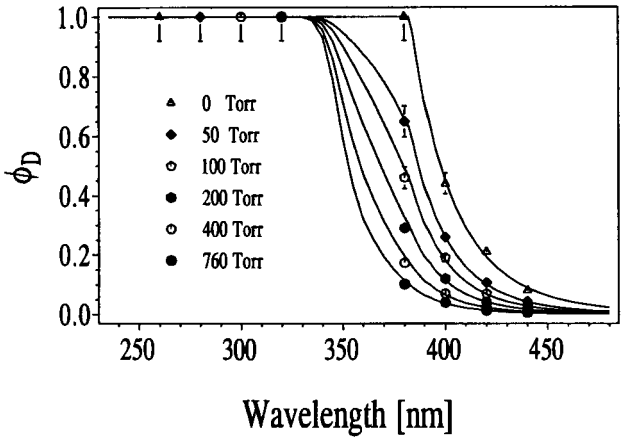

Figure 10. Quantum yields of dissociation as a function of wavelength for various pressures. Symbols: calculated according to eq 11 using the coefficients given in Table 4; lines: calculated according to eqs 11, 17, 18.

TABLE 4: Coefficients of Quantum Yield of Dissociation According to Equation 11

λ[nm]	ϕ_0	k'_D [Torr]	k'_X [Torr]
380	1.10 ± 0.14	78 ± 9	-7 ± 8
400	0.47 ± 0.09	31 ± 4	41 ± 12
420	0.21 ± 0.06	10 ± 1	32 ± 6
440	0.08 ± 0.02	4 ± 0.3	46 ± 7

TABLE 5: Relative Errors of the Quantum Yield of Dissociation

error source	relative error
photolysis rate (d[Prod]/dt])	$\pm$7%
actinometry (I_0)	$\pm$10%
adsorption cross section (σ)	$\pm$6%
concentration of MG ([MG])	$\pm$6%
dark loss of MG (k_{dark})	$\pm^{5}_{0}$%
coefficients (δ, ϵ)	$\pm$5%
optical resolution ($\Delta\lambda$)	$\pm^{0}_{6}$%
quantum yield (ϕ_D)	$\pm$17%

18, the quantum yield of photodissociation can be specified as a function of wavelength and pressure (Figure 10), as required for the calculation of the lifetime of MG. In the range between 335 and 345 nm, these functions were interpolated to form a smooth transition to $\phi_D = 1$ of the short-wavelength band.

The relative standard deviations of the quantum yields as a function of wavelength were determined to be 7%, possible systematic errors introduced by uncertainties of the coefficients δ and ϵ are thought to be less than 5%. The finite optical resolution (8.5 nm) leads to an overestimation of the quantum yields of not more than 6%. Summarizing all statistical as well as systematical errors, shown in Table 5, results in a relative uncertainty of the quantum yields determined of $\Delta\phi_D/\phi_D = \pm 17\%$.

Quantum Yields of Reaction R10. The quantum yields ϕ_R of the reaction of electronically excited MG with ground-state MG (R10) were calculated from experimental data using eq 16.

The results of the experiments performed in synthetic air are displayed as a function of total pressure in Figure 11 and can be empirically described by a function analogous to eq 20.

The dependence of the quantum yields ϕ_R of MG concentration, determined at 380 and 440 nm, all other experimental conditions kept constant, is shown in Figure 12. The experimental data can be represented by saturation functions of the

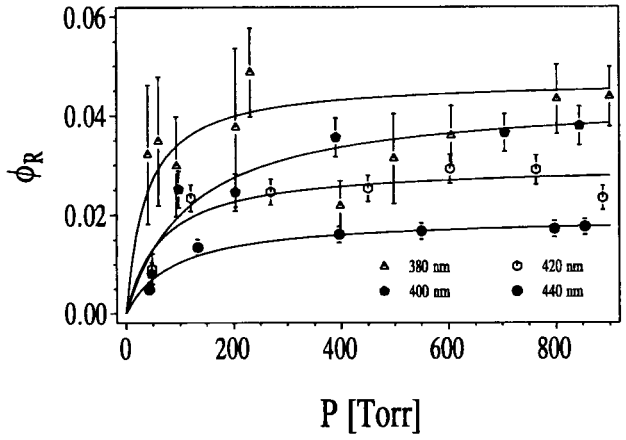

Figure 11. Quantum yields of R10 as a function of total pressure obtained in synthetic air. Symbols: calculated from experimental data according to eq 16; curves: fit according to eq 20.

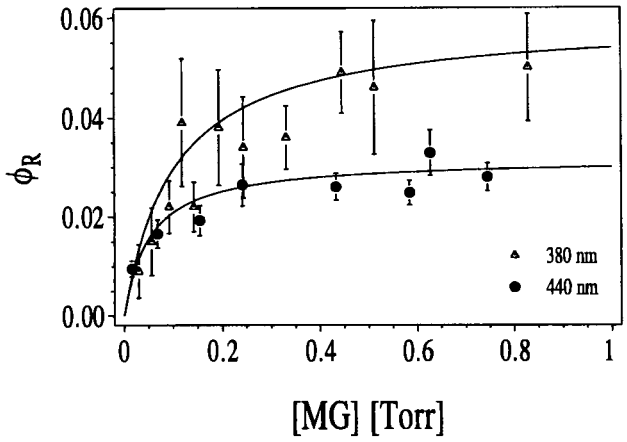

Figure 12. Quantum yields of R10 as a function of MG concentration (380 nm: $P = 400$ Torr, $[O_2] = 90$ Torr; 440 nm: $P = 760$ Torr, $[O_2] = 150$ Torr). Symbols: calculated from experimental data according to eq 16; curves: fit according to eq 23.

type

$$\phi_R \sim \frac{k_{MG}[MG]}{k_{\Sigma MG}[MG] + k_i} = \frac{K_{MG}}{1 + k'_i/[MG]} \qquad (19)$$

where $(k_{MG})[MG]$ represents the effective rate of R10, $k_{\Sigma MG}$ the sum of all quenching processes dependent on [MG], and k_i all deactivation processes obeying first- as well as pseudo-first-order kinetics. The ratio $k_{MG}/k_{\Sigma MG} = K_{MG}$ gives the limit of the yield at high concentrations.

The effect of O_2 partial pressure on ϕ_R was investigated under conditions of constant MG partial and constant total pressure at 380 and 440 nm. The results shown in Figure 13 can also be represented by a saturation function,

$$\phi_R \sim \frac{k_{O_2}[O_2]}{k_{\Sigma O_2}[O_2] + k_T} = \frac{K_{O_2}}{1 + k'_T/[O_2]} \qquad (20)$$

with K_{O_2} giving the limit of ϕ_R at high O_2 partial pressure. By comparison of the plots in Figures 12 and 13, it can be observed that the limits of ϕ_R reached at large [MG] and $[O_2]$, respectively, show nearly the same values. The interpretation of these results requires product-forming as well as deactivation pathways of the reactive state under participation of MG as well as oxygen.

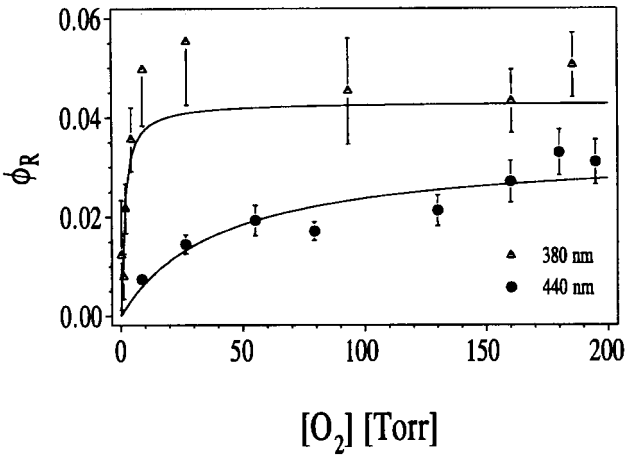

Figure 13. Quantum yields of R10 as a function of O_2 partial pressure (380 nm: $P = 400$ Torr, [MG] = 0.25 Torr; 440 nm: $P = 760$ Torr, [MG] = 0.25 Torr). Symbols: calculated from experimental data according to eq 16; curves: fit according to eq 23.

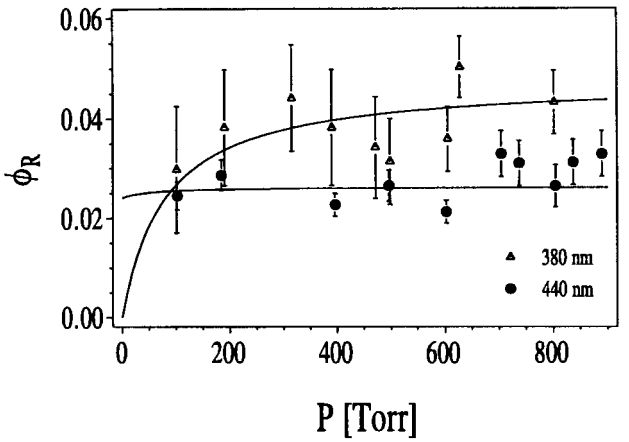

Figure 14. Quantum yields of R10 as a function of total pressure obtained under constant O_2 and MG partial pressure. (380 nm: $[O_2]$ = 150 Torr, [MG] = 0.20 Torr; 440 nm: $[O_2]$ = 150 Torr, [MG] = 0.25 Torr). Symbols: calculated from experimental data according to eq 16; curves: fit according to eq 23.

Quantum yields as a function of total pressure, at constant MG and O_2 partial pressure, are displayed in Figure 14. Within experimental error no pressure effect could be observed. Therefore the pressure effect observed in the experiments performed in synthetic air (Figure 11) has to be interpreted as an O_2 partial pressure dependence.

The errors indicated by the bars in Figures 11−14 represent the weighted sum of $\Delta(d[CO]/dt)$ and $\Delta(d[HCHO]/dt)$. Systematic errors caused by the uncertainties of δ and ϵ do not change the calculated values of ϕ_R by more than 10%, while the shape of the curves remains unaffected.

In the following section these experimental findings are discussed with respect to the photophysics of dicarbonyl compounds.

Photochemical Model

The photochemistry of MG in the presence of O_2 is described by a photodissociation mechanism according to P1′.

$$CH_3COCHO \xrightarrow{h\nu} \xrightarrow{O_2,M} CH_3COO_2 + HO_2 + CO \quad (P1')$$

For absorptions in the short-wavelength band ($\lambda < 340$ nm) dissociation quantum yields of unity, independent of photon energy as well as pressure, were obtained. In the second absorption band ($\lambda > 340$ nm) dissociation quantum yields decrease with increasing wavelength and increasing total pressure, obeying the Stern−Volmer relationship (eq 11). Further, a chemical reaction of electronically excited MG with MG in the ground state (R10) was proposed.

$$[CH_3COCHO]^* + HCOCOCH_3 \rightarrow CH_3CO + HCHO + CO + CH_3CO \quad (R10)$$

TABLE 6: Quantum Yields of Intersystem Crossing

λ[nm]	$\frac{k_{IX}}{k^+}$ (ref 32)	$\phi_{X_0} = \frac{k'_X}{k'_D + k'_X}$ (this work)	λ[nm]
		0	380
401	0.66 ± 0.09	0.55 ± 0.05	400
420	0.77 ± 0.11	0.76 ± 0.02	420
442	0.99 ± 0.14	0.92 ± 0.01	440

This mechanism may be discussed with respect to the previously published studies dealing with the photophysics of MG of van der Werf et al.[32] and Coveleskie and Yardley.[28,33,34] They investigated the fluorescence and phosphorescence of MG at excitation wavelengths between 398 and 455 nm. Their results relevant to this work are summarized as follows:

(i) Methylglyoxal in its first electronically excited state (S_1) undergoes fast intersystem crossing to a triplet state with rates in the order of magnitude of 10^7 s^{-1}.[32,34]

(ii) The collisionless quantum yields of intersystem crossing (k_{ST}/k^+, with k_{ST} representing the rate coefficient of intersystem crossing and k^+ the sum of all monomolecular deactivation processes) obtained by van der Werf et al.[32] are in excellent agreement with the quantum yields of monomolecular deactivation extrapolated to zero pressure ($\phi_{X_0} = k_X/(k_X + k_D) = 1 - \phi_0$, Table 6). Hence k_D and k_X can be identified as rate coefficients of dissociation and intersystem crossing to a nondissociative triplet state, respectively. Moreover, these processes can be regarded as the only significant monomolecular dissipation pathways of vibrationally excited MG in the S_1 state.

(iii) The results at 380 nm must be regarded as somewhat different. The quantum yield of dissociation, extrapolated to zero pressure (ϕ_0), is unity. Since it cannot be expected that intersystem crossing becomes negligible at this wavelength,[35] it is concluded that the corresponding triplet state is also dissociative.

(iv) Collisional quenching of vibrationally excited triplets ($c^q \approx 10^7$ s^{-1} $Torr^{-1}$) is orders of magnitudes faster than the competing first-order processes ($k_T < 10^6$ s^{-1}).[32]

(v) No experimental data concerning the triplet quenching of MG by oxygen is available. Nevertheless, the thermalized phosphorescence of the homologous biacetyl is strongly quenched by O_2 with a rate of 2.8×10^4 s^{-1} $Torr^{-1}$.[36] Hence, triplet MG must also be considered to be efficiently electronically deactivated by oxygen.

(vi) Intersystem crossing from the thermalized S_1 state ($k_{IX}^{therm} = 4.9 \times 10^7$ s^{-1}) is orders of magnitudes faster than fluorescence ($k_{Fluorescence} \approx 10^5$ s^{-1}).[33]

Following these arguments, the conclusions can be drawn that under the experimental conditions employed in this work, all molecules in triplet states are thermalized and all nondissociating molecules undergo intersystem crossing, reaching the thermalized triplet states. Therefore, the states responsible for the reaction of electronically excited MG should be thermalized triplets and the experimentally determined quantum yield of this

reaction should be proportional to the triplet quantum yield (ϕ_T), which is equivalent to the quantum yield of nondissociation ($1 - \phi_D$).

$$\phi_R(\lambda, P) \sim \phi_T(\lambda, P) \tag{21}$$

$$\phi_T(\lambda, P) = 1 - \phi_D(\lambda, P) \tag{22}$$

This relationship is shown by the lines in Figure 14, with the values of $1 - \phi_D$ calculated from the coefficients given in Table 4.

In order to explain the experimentally observed photon energy, $[O_2]$ as well as [MG] dependence of the quantum yield ϕ_R, detailed information concerning the chemical and physical properties of the involved triplet states of MG is necessary. The properties of triplet MG and the homologous biacetyl ($CH_3COCOCH_3$), respectively, were examined by several experimental as well as theoretical studies. The results needed for the discussion of this work are summarized as follows:

(i) The CO quantum yield of biacetyl at 436 nm increases with O_2 partial pressure, the yields were described by a saturation function ($\phi_{CO} = ((0.07 \pm 0.03)\ s^{-1})/(1 + (0.012 \pm 0.002)\ s^{-1}\ Torr^{-1})/[O_2])$.[37] A similar behavior was observed for the CO quantum yield of acetaldehyde (313 nm).[38] These results were interpreted in terms of a bimolecular interaction of oxygen with triplet biacetyl and acetaldehyde, respectively, following product formation.

(ii) Molecular orbital considerations on the basis of biacetyl with C_{2h}-symmetry show the existence of two triplet states that can be reached by intersystem crossing from the first excited singlet. The first triplet, lying about 3000 cm^{-1} below the singlet,[33] is assigned to be of $^3A_u^I$, the second of $^3B_g^{II}$ symmetry.[27]

(iii) However, there exists some disagreement concerning the energy differences of these states. Drent et al. assume the energy difference of both states to be as small as 2500 cm^{-1} (29 kJ/mol),[39] while Coveleskie and Yardley estimate the $^3B_g^{II}$ state lying at 27000 cm^{-1}, inaccessible for excitation wavelengths longer than 370 nm.[33]

(iv) An experimental indication to the population of two different triplet states can be taken from the biexponential time profiles of the slow fluorescence of MG, initiated by reverse intersystem crossing which was observed at all wavelengths investigated.[32]

The experimentally obtained dependence of ϕ_R on MG and oxygen partial pressure as well as photon energy can be brought into consistency with the known physical properties of electronically excited MG by the photochemical model described below.

The increase of ϕ_R with O_2 partial pressure (Figure 13, eq 20) requires the participation of O_2 in product formation. We propose that a minor portion of the collisions of triplet MG with O_2 leads to some reactive intermediate (k_{O_2}), not identified, undergoing further collisions with MG, yielding the reaction products according to R10 (k_{MG}). This assumes that the major amount of triplets is electronically deactivated by oxygen ($k_{\Sigma O_2}$) or other first-order kinetic processes (k_T) like phosphorescence, internal conversion, or intersystem crossing.

In order to explain the [MG] dependence of ϕ_R as displayed in Figure 12 (eq 19), besides a product promoting pathway via R10 (k_{MG}), competitive deactivation of the assumed intermediate by first-order (k_i) as well as MG dependent ($k_{\Sigma MG}$) kinetic processes is suggested.

Following these considerations, an analytical expression for ϕ_R which combines eqs 19−22 as displayed in Figures 12, 13, and 14 can be given,

$$\phi_R = (1 - \phi_D)\left(\frac{k_{O_2}[O_2]}{k_{\Sigma O_2}[O_2] + k_T}\right)\left(\frac{k_{MG}[MG]}{k_{\Sigma MG}[MG] + k_i}\right)$$

$$= (1 - \phi_D)\left(\frac{K_R}{(1 + k'_T/[O_2])(1 + k'_i/[MG])}\right) \tag{23}$$

where $K_R = (k_{O_2}/k_{\Sigma O_2})(k_{MG}/k_{\Sigma MG}) = K_{O_2}K_{MG}$, and all coefficients have to be considered as functions of the wavelength as given in Table 7.

TABLE 7: Coefficients of the Quantum Yield of R10[a]

λ[nm]	K_R	k'_i [Torr]	k'_T [Torr]
380	0.072 ± 0.01	1.45 ± 0.7	0.10 ± 0.05
440	0.040 ± 0.005	40 ± 18	0.05 ± 0.03

[a] The assigned errors represent one standard deviation obtained by least-squares fitting.

For explanation of the observed wavelength dependence of ϕ_R, the participation of two distinct triplet states, populated with different energy-dependent probabilities is assumed. Therefore the coefficients entered in Table 7 have to be considered as some mean values of the different states involved.

The thermodynamics of R10a require triplet energies corresponding to a threshold wavelength of 434 nm, whereas the formation of acetylperoxy instead of acetyl radicals diminishes this threshold to 935 nm.

$$[CH_3COCHO]^* + HCOCOCH_3 \rightarrow CH_3CO + HCHO + CO + CH_3CO \quad \text{(R10a)}$$

$$[CH_3COCHO]^* + HCOCOCH_3 \xrightarrow{O_2} CH_3COO_2 + HCHO + CO + CH_3CO \quad \text{(R10b)}$$

Therefore, the participation of oxygen might thermodynamically open the product formation channel (R10b). However, a mechanistic interpretation might be too speculative. A further confirmation of the proposed reaction mechanism can be obtained by experiments using partially deuterated methylglyoxal (CH_3COCDO). Reaction R10 yields exclusively deuterated formaldehyde (DCDO) if the exchange of deuterium between ground-state molecules is sufficiently slow. The reaction rate is expected to be reduced according to the kinetic isotope effect.

Comparison to Recent Investigations

The quantum yields of CO and HCHO determined in this work agree only qualitatively with those obtained by Raber and Moortgat[18,19] and Staffelbach et al.,[20] respectively, as outlined in Table 8.

Raber and Moortgat[18,19] observed nonlinear product−concentration time profiles. The ratio $\Delta[CO]/\Delta[MG]$ increased linearly with photolysis time, while the ratio $\Delta[HCHO]/\Delta[MG]$ slightly decreased with time (Table 8). These observations could not be explained by their kinetic model, consisting of the reactions as given in Table 2 with slightly different rate constants and reaction of MG with HO_2 (R11) included.

$$CH_3COCHO + HO_2 \rightleftharpoons CH_3COCHO\text{-}O_2H \rightarrow \text{Products} \quad \text{(R11)}$$

Possibly, secondary chemical processes occurred, caused by higher concentrations of radical and molecular intermediates, since their photon flux was about two orders of magnitude higher than in this work. Wall effects are not mentioned.

TABLE 8: Comparison to Recent Studies of the Photochemistry of MG

Raber[18]	P [Torr]	Δ[CO]/Δ[MG]	Δ[HCHO]/Δ[MG]	ϕ_{MG}[a]	ϕ_D[d]
$\lambda = 275-380$ nm	54	0.85−1.6	0.28−0.22	1.11 ± 0.03	0.94 ± 0.04
	146	0.85−1.3	0.35−0.22	1.07 ± 0.01	0.90 ± 0.03
	220	1.00−2.0	0.31−0.18	0.99 ± 0.05	0.87 ± 0.05
	400	0.90−1.1	0.38−0.30	0.95 ± 0.05	0.82 ± 0.04
	600	0.30−1.0	0.27−0.20	0.86 ± 0.04	0.75 ± 0.03
	760	0.65−0.9	0.28−0.21	0.72 ± 0.02	0.64 ± 0.03
$\lambda = 390-470$ nm	57	0.63−1.0	0.20−0.16	0.51 ± 0.04	0.41 ± 0.04
	148	0.44−0.55	0.32−0.22	0.31 ± 0.03	0.28 ± 0.01
	600	0.18−0.35	0.28−0.21	0.26 ± 0.03	0.22 ± 0.02
	760	0.28−0.31	0.35−0.22	0.26 ± 0.04	0.23 ± 0.02
Staffelbach[20]	P [Torr]	Δ[CO]/Δ[MG]	Δ[HCHO]/Δ[MG]	ϕ_{MG}[a]	ϕ_D[d]
$\lambda = 410-418$ nm	760	*b*	*b*	$2(\phi_{MG} - \phi_{R11})$	0.005
$\lambda = 355-480$ nm	760	<0.78	0.51 ± 0.06		0.055
$\lambda = 240-420$ nm	760	<1.44	0.30 ± 0.06		0.14
this work	P [Torr]	$\phi_{CO'}/\phi_D$	ϕ_{HCHO}/ϕ_D	ϕ_{MG}[a]	$\phi_{CO'} - \phi_R$
all λ	all P	1.0 ± 0.1	0.19 ± 0.02	*c*	
$\lambda = 420$ nm	760				0.013 ± 0.03

[a] $\phi_{MG} = -(d[MG]/dt)/(\int I_0\, d\lambda\, \sigma\, [MG])$. [b] Not specified. [c] Not determined. [d] $\phi_D = (\phi_{MG} - \phi_{R11})$.

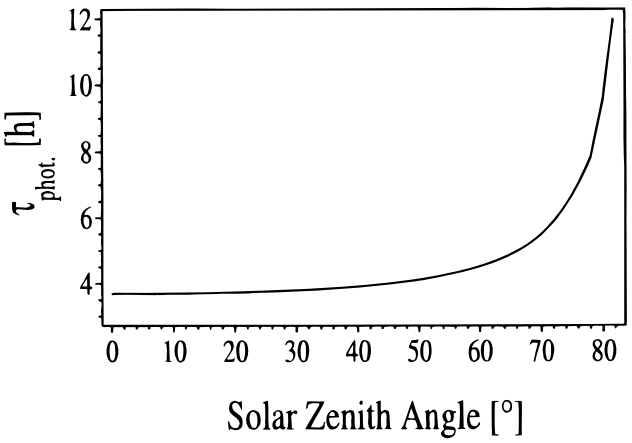

Figure 15. Atmospheric lifetime of MG due to photolysis as a function of solar zenith angle ($z = 0.5$ km, $P = 760$ Torr, albedo = 0.2).

Staffelbach et al.[20] studied the wavelength dependence of the photolysis using broad-band cut-off filters specified by their threshold wavelengths. The pressure dependence of the quantum yield was not investigated, all experiments were performed at 760 Torr. The CO quantum yields determined have to be considered as upper limits. The results of their model calculations could not be reproduced with the given rate coefficients; e.g., the model calculations resulted in a carbon balance of 100%, although the postulated product CH_3O_2H was not included and HCHO yields higher than 60% per molecule of MG removed were calculated.

Their experimental results are not in agreement with this work. Their ratio Δ[CO]/Δ[MG] is significantly lower and Δ-[HCHO]/Δ[MG] significantly higher than the quantum yields determined in this study (Table 8).

In a further experiment Staffelbach et al.[20] investigated the photolysis of a mixture of H_2, O_2, N_2, MG, and Cl_2 in order to determine the rate of the reaction of MG with HO_2 (R11). The examination of the stable products resulted in an effective rate constant of $k_{11} = (1.4 \pm 0.5) \times 10^{-15}$ cm^3 molecule^{-1} s^{-1}, leading to the conclusion that during the photolysis of MG half of the removal of MG is the result of the reaction with HO_2 (R11). Their photolysis quantum yield obtained in the wavelength range between 410 and 418 nm is about half as large as the CO quantum yield found at 420 nm in this work. Both results would be compatible if one would assume that reaction R11 is negligibly slow, in contradiction to the findings of Staffelbach et al. There is no explanation for these discrepancies. However, a direct determination of the rate coefficient of R11 would give a deeper understanding of the photochemistry of MG.

Atmospheric Lifetime

The atmospheric photodissociation coefficient (J) is defined as the integral of the solar flux per unit wavelength (I_0) as a function of height (z), the solar zenith angle (θ), the absorption cross section (σ), and the quantum yield (ϕ) of the considered process over the atmospherically relevant wavelength range. The atmospheric lifetime due to photolysis (τ_{phot}) is the reciprocal of the photodissociation coefficient.

$$J(P, T, z, \theta) = \int I_0(\lambda, z, \theta)\, \sigma(\lambda, P, T)\, \phi(\lambda, P, T)\, d\lambda$$

$$\tau_{phot} = J^{-1}$$

The radiation model is related to that of Luther and Gelinas.[40] The solar photon flux is incrementally calculated for a standard atmosphere with respect to the extraterrestrial spectrum, absorptions due to N_2, O_2, O_3, and NO_2, multiple scattering, and a constant albedo. The calculations of the photodissociation coefficient were performed for the height increment between 0 and 1 km (760 Torr) and an albedo of 0.2, using the absorption cross sections given by Meller et al.[10] and the quantum yields of dissociation given by eqs 11, 17, and 18 as shown in Figure 10. Atmospherically, only photodissociation of MG is relevant, the suggested reaction of triplet CH_3COCHO is of no importance due to the low concentrations of reactants. The results of the model calculations for $z = 0.5$ km as a function of the zenith angle are shown in Figure 15. For an angle of 50° one obtains a lifetime due to photolysis of

$$\tau_{phot} = 4.1 \text{ h} \pm 0.7 \text{ h}$$

with respect to the error of the quantum yield ϕ_D.

The lifetime due to OH reaction is calculated to be 16 h for an OH concentration of 1×10^6 molecules cm^{-3} and a room-temperature rate coefficient of $k_3 = 1.3 \times 10^{-11}$ cm^3 molecule^{-1} s^{-1}.[21] Hence, OH reaction is of minor importance for the

degradation of tropospheric MG. The photolysis lifetime of 2 h given by Plum et al.[23] is based on experiments using an unfiltered Xe arc lamp in order to simulate the solar spectrum. Raber and Moortgat[19] reported a value of 0.6 h based on a wavelength-independent quantum yield of 0.23, obtained with a light source showing a broad emission between 390 and 470 nm. Their results are possibly affected by systematic errors. The results of Staffelbach et al. (2.7 h $\pm$ 0.7 h)[20] are in good agreement with those of this work. They assume a quantum yield of dissociation linearly decreasing with wavelength (ϕ_D(300 nm) = 0.45, ϕ_D(430 nm) = 0), assuming that only about half of the MG removed in their experiments is due to photolysis. This function results in higher yields in the atmospherically effective window between 420 and 370 nm.

Finally, in order to complete our understanding of the fate of atmospheric MG, information concerning its dry and wet deposition is necessary.

References and Notes

(1) Killus, J. P.; Whitten, G. Z. *Environ. Sci. Technol.* **1984**, *18*, 142.

(2) Lloyd, A. C.; Atkinson, R.; Lurmann, F. W.; Nitta, B. N. *Environ. Sci. Technol.* **1983**, *17*, 1931.

(3) Paulson, S. E.; Flagan, R. C.; Seinfeld, J. H. *Int. J. Chem. Kinet.* **1992**, *24*, 79.

(4) Kamens, R. M.; Gery, M. W.; Jeffries, H. E.; Jackson, M.; Cole, E. I. *Int. J. Chem. Kinet*. **1982**, *14*, 955.

(5) Niki, H.; Maker, P. D.; Savage, C. M.; Breitenbach, L. P. *Environ. Sci. Technol*. **1983**, *17*, 312 A.

(6) Paulson, S. E.; Flagan, R. C.; Seinfeld, J. H. *Int. J. Chem. Kinet.* **1992**, *24*, 79.

(7) Tuazon, E. C.; Atkinson, R. *Int. J. Chem. Kinet.* **1990**, *22*, 591.

(8) Tuazon, E. C.; Atkinson, R. *Int. J. Chem. Kinet.* **1989**, *21*, 1141.

(9) Atkinson, R.; Aschmann, S. M.; Winer, A. M.; Pitts, J. N., Jr. *Int. J. Chem. Kinet*. **1981**, *13*, 1133.

(10) Meller, R.; Raber, W.; Crowley, J. N.; Jenkin, M. E.; Moortgat, G. K. *J. Photochem. Photobiol., A* **1991**, *62*, 163.

(11) Jenkin, M. E.; Cox, R. A.; Emrich, M.; Moortgat, G. K. *J. Chem. Soc., Faraday Trans.* **1992**, *89*, 2983.

(12) Tuazon, E. C.; Atkinson, R.; MacLeod, H.; Biermann, H. W.; Winer, A. M.; Carter, W. P. L.; Pitts, J. N., Jr. *Environ. Sci. Technol.* **1984**, *18*, 981.

(13) Tuazon, E. C.; MacLeod, H.; Atkinson, R.; Carter, W. P. L. *Environ. Sci. Technol.* **1986**, *20*, 383.

(14) Seuwen, R.; Warneck, P. *Int. J. Chem. Kinet*. **1996**, *28*, 315.

(15) Lightfoot, P. D.; Cox, R. A.; Crowley, J. N.; Destiau, M.; Hayman, G. D.; Jenkin, M. E.; Moortgat, G. K.; Zabel, F. *Atmos. Environ.* **1992**, *26A*, 1805.

(16) Munger, J. W.; Jacob, D. J.; Daube, B. C.; Horowitz, L. W.; Keene, W. C.; Heikes, B. G. *J. Geophys. Res.* **1995**, *100*, 9325.

(17) Lee, Y. N.; Zhou, X.; Hallock, K. *J. Geophys. Res*. **1995**, *100*, 25933.

(18) Raber, W. PhD. Thesis, Johannes Gutenberg-University, Mainz, Germany, 1992.

(19) Raber, W.; Moortgat, G. K. In *Progress and Problems in Atmospheric Chemistry*; Barker, J., Ed.; Singapore, 1996; p 318.

(20) Staffelbach, T. A.; Orlando, J. J.; Tyndall, G. S.; Calvert, J. G. *J. Geophys. Res*. **1995**, *100*, 14189.

(21) Tyndall, G. S.; Staffelbach, T. A.; Orlando, J. J.; Calvert, J. G. *Int. J. Chem. Kinet*. **1995**, *27*, 1009.

(22) DeMore, W. B.; Sander, S. P.; Golden, D. M.; Molina, M. J.; Hampson, R. F.; Kurylo, M. J.; Howard, C. J.; Ravishankara, A. R.; Kolb, C. E. Chemical Kinetics and photochemical data for use in stratospheric modelling, Evaluation number 11, JPL Publication 94-26, 1994.

(23) Plum, C. N.; Sanhueza, E.; Atkinson, R.; Carter W. P. L.; Pitts, J. N., Jr. *Environ. Sci. Technol.* **1983**, *17*, 479.

(24) Atkinson, R.; Baulch, D. L.; Cox, R. A.; Hampson, R. F., Jr.; Kerr, J. A.; Rossi, J. M.; Troe, J. *J. Phys. Chem. Ref. Data* **1997**, *26*, (3), 521−1011.

(25) Wright, B. W.; Lee, M. L.; Graham, S. W.; Phillips, L. V.; Hercules, D. M. *J. Chromatogr*. **1980**, *199*, 355.

(26) Maric, D.; Burrows, J. P.; Meller, R.; Moortgat, G. K. *J. Photochem. Photobiol., A* **1993**, *70*, 205.

(27) Drent, E.; Kommandeur, J. *Chem. Phys. Lett.* **1972**, *14*, 321.

(28) Coveleskie, R. A.; Yardley, J. T. *Chem. Phys*. **1975**, *9*, 277.

(29) Facsimile, Release H010, Version 101010, United Kingdom Atomic Energy Authority, Harwell, 1987.

(30) Benson, S. W. *Thermochemical Kinetics*; New York, 1976.

(31) McMillan, G. R.; Calvert, J. G.; Pitts, J. N., Jr. *J. Am. Chem. Soc.* **1994**, *86*, 3602.

(32) van der Werf, R.; Schutten, E.; Kommandeur, J. *Chem. Phys*. **1976**, *16*, 151.

(33) Coveleskie, R. A.; Yardley, J. T. *J. Am. Chem. Soc*. **1975**, *97*, 1667.

(34) Coveleskie, R. A.; Yardley, J. T. *Chem. Phys*. **1976**, *13*, 441.

(35) van der Werf, R.; Kommandeur, J. *Chem. Phys.* **1976**, *16*, 125.

(36) Kaskan, W. E.; Duncan, A. B. F. J. *Chem. Phys*. **1950**, *18*, 427.

(37) Padnos, N.; Noyes, W. A. *J. Phys. Chem.* **1964**, *68*, 464.

(38) Weaver, J.; Meagher, J.; Heicklen, J. *J. Photochem*. **1976**, *6*, 111.

(39) Drent, E.; van der Werf, R.; Kommandeur, J. *J. Phys. Chem*. **1973**, *59*, 2061.

(40) Luther, F. M.; Gelinas, R. J. *J. Geophys. Res*. **1976**, *81*, 1125.

(41) Bauer, D.; Crowley, J. N.; Moortgat, G. K. *J. Photochem. Photobiol., A* **1992**, *65*, 329.

(42) Dagaut, P.; Wallington, T. J.; Kurylo, M. J. *J. Phys. Chem.* **1988**, *92*, 3836.

(43) Wallington, T. J.; Japar, S. M. *Chem. Phys. Lett*. **1990**, *166*, 495.

(44) Kaiser, E. W.; Rimai, L.; Wallington, T. J. *J. Phys. Chem.* **1989**, *93*, 4094.

(45) Roehl, C. M.; Bauer, D.; Moortgat, G. K. *J. Phys. Chem.* **1996**, *100*, 4038.

(46) Bauer, D. PhD. Thesis, Johannes Gutenberg-University, Mainz, Germany, 1996.